

Article

Investigation of the Wind Resource Assessment over 2D Continuous Rolling Hills Due to Tropical Cyclones in the Coastal Region of Southeastern China

Mingming Zhang * and Mengting Liu

Institute of Engineering Thermophysics, Chinese Academy of Sciences, Beijing 100190, China;
E-Mail: liumengting@iet.cn

* Author to whom correspondence should be addressed; E-Mail: mmzhang@mail.etp.ac.cn;
Tel./Fax: +86-10-8254-3023.

Received: 9 December 2013; in revised form: 15 February 2014 / Accepted: 18 February 2014 /
Published: 20 February 2014

Abstract: The effect of tropical cyclones on the turbulent flow over 2D continuous rolling hills was numerically investigated based on a field test analysis of the coastal region of Southeast China. A computational fluid dynamics (CFD) method was first developed and verified using previously published experimental results. Then two typical beneficial and destructive cyclone cases were studied above different locations of the hills. Results showed that the continuous hilly flow was much more drastic and variable than previously reported normal wind; the mean and turbulent magnitudes became the strongest around the hill top, with the maximum speed-up ratio, turbulence intensity and gust-speed ratio of 1.1, 0.32 and 1.6; the flow over lower hill was greatly affected by the nearby higher hills; the mean and fluctuating quantities were mostly smaller than the corresponding single hill case. These phenomena were considered to be related with the rather strong detachment and attachment of the cyclone flow around the two hills. In addition, the mean and fluctuating wind velocities were found to be underestimated by at least 20% if the widely accepted IEC standard equations were utilized, suggesting the necessity to supplement the field test analysis in the standard for more reasonable wind resource evaluation within the Southeast China coastal area.

Keywords: tropical cyclone; continuous rolling hill; wind evaluation; micro-sitting; computational fluid dynamics (CFD)

1. Introduction

It is well known that the wind resources in the coastal area of Southeast China are the most abundant in the country, with an average wind power density of more than 300 W/m^2 and a utilization hour of more than 6000 h. The economy is rather developed in the region, but the electric power shortage problem is becoming increasingly serious, which has led to the fast development of wind energy resources in recent years. However, this region is often subject to strong tropical cyclones, posing a serious threat to the normal construction of wind farms. Considering the Beaufort scale [1] and the common cut-out wind speed of the commercial wind turbines ($\approx 25 \text{ m/s}$) [2], the cyclones may be generally classified into beneficial, defensive and destructive cases, respectively, summarized in Table 1. Here the maximum wind velocity corresponds to the one at a nominal hub height of 70 m.

Table 1. Classification of tropical cyclones.

Classification	Beaufort scale		Wind scale	Maximum velocity at hub height (=70 m) (m/s)
	Tropical cyclone	Centre maximum velocity (m/s) at 10 m		
Beneficial	Tropical depression	10.8–17.1	6–7	15.3–24.3
Defensive	Tropical storm	17.2–24.4	8–9	24.4–32.0
	Severe tropical storm	24.5–32.6	10–11	32.1–42.8
Destructive	Typhoon	32.7–41.4	12–13	42.9–54.4
	Severe typhoon	41.5–50.9	14–15	54.5–66.8
	Super typhoon	51.0–61.2 or above	16–17 or above	66.9–80.4 or above

Generally speaking, beneficial cyclones (wind scale 6–7) can be very profitable for offshore wind farms. For example, the electricity generated by the beneficial cyclone “Morak” during 6 days accounted for 2/3 of total electricity of the wind farms in one month when it passed by Zhejiang and Jiangsu Provinces in 2009. In contrast, a destructive cyclone (wind scale greater or equal than 10) may frequently destroy wind farm components such as blades and towers, and even the whole turbine system, resulting in a great loss to the local wind developers. Typical examples include typhoon “Cuckoo” in 2003, typhoon “Pearl” in 2006, typhoon “Saomai” in 2006 and Typhoon “Megi” in 2010, and so on. Therefore, to fully utilize beneficial cyclones as well as guard against the defensive and the destructive ones, in depth systematic research on the characteristics of turbulent flow need to be conducted. Nevertheless, due to lack of well-documented field test data, little work has been done in the past.

On the other hand, large land areas in the Chinese coastal region are covered by continuous rolling hills, causing flow separation behind hills and recirculation in valleys, which may further enhance the influence of tropical cyclones on the construction and the operation of a wind farm. For instance, according to news reports, a total of 13 turbines in the Shanwei wind farm in Guangdong Province were essentially destroyed by the typhoon “Cuckoo” in 2003, among which nine turbines were located on rolling hills with relative high altitude. This makes it very necessary to analyze the role that this kind of complex terrain plays on the cyclone wind flow.

Previously, under normal wind conditions, many researchers have focused their interests on 2D and 3D continuous or single terrain cases to understand the fundamental flow phenomena, and this work can be roughly divided into experimental tests and numerical simulations. For the former, experiments

were often carried out in wind tunnels to measure the distributions of mean and fluctuating magnitudes, e.g., mean velocity, fractional speed-up ratio, turbulence intensity, turbulent kinetic energy and Reynolds stress, using Particle Image Velocimetry (PIV), hot wires or Pitot tubes, *etc.* In this way, one may study how the complex terrains affect the local atmospheric boundary layer [3–10]. In respect of numerical work, most research efforts have been made on turbulence modeling, surface roughness, boundary condition and grid generation to guarantee the accuracy and efficiency of the computational fluid dynamics (CFD) computation on terrain effect [11–17]. Nevertheless, to our knowledge no research work concerning the tropical cyclone case has been reported before.

Furthermore, the design of the modern wind turbines mostly abides by some international standard, *i.e.*, IEC-61400-1 [18] (hereafter abbreviated as IEC standard), to make the wind turbine resist the loads with a defined survival probability. But this standard was generally built based on the European and North American conditions and did not include the experiences from the areas with extreme phenomena such as tropical cyclones, leading to a certain degree of errors in the turbine design process if fully followed [19]. In practice, the design of wind turbines that can survive at the high wind speeds caused by a tropical cyclone is no problem and the challenge is to cost optimize the wind turbine design for sites with cyclone exposure risk. For this purpose, we need appropriate data to modify or extend the existing methodologies used in the IEC standard so that the designs could be optimized to the specific wind conditions in the cyclone risk areas.

To cover the aforementioned points, systematic numerical and experimental studies need to be conducted to examine the effect of the tropical cyclones on the turbulent flow over complex terrains within the southeast coastal area in China. In the first stage, the mean and fluctuating characteristics of turbulent cyclone flow over 2D double hills were numerically investigated in this paper. Considering its complicated situation, the experimental work will be carried out in the near future. To this end, we first developed a CFD method and then verified it by comparing the numerical results with the experimental ones by Kim *et al.* [4]. After that, the developed CFD arithmetic was utilized to assess the flow field over double hills under typical beneficial and destructive cyclone conditions, based on the analysis of the field test data around the Chinese southeast coastal area. In addition, we also made a comparison with the computation results based on the IEC standard to comment on the differences and the improvements as well. In doing so, we hope to provide helpful information for the development of the coastal wind energy under the influence of tropical cyclones in China, e.g., micro-siting, turbine design and safety management, *etc.*

2. Development of Computational Fluid Dynamics (CFD) Method

The CFD method was built on the basis of the Reynolds-averaged Navier-Stokes equations using the commercial FLUNT code. In order to simulate well the concerned atmospheric boundary layer, a classical two-equation high Reynolds number k - ε model with five improved empirical constants, *i.e.*, C_μ , $C_{\varepsilon 1}$, $C_{\varepsilon 2}$, σ_k and σ_ε , equal to 0.03, 1.21, 1.92, 1.00 and 1.30, respectively, which was utilized to obtain the eddy-viscosity for the RANS simulation in the reference [20], was employed in the present CFD computation.

Deploying a method similar to that of Zhang [21], a user-defined wall function for the near-wall treatment was designed to solve the matching between the roughness height and 1st layer's cell height.

Working with the $k-\varepsilon$ turbulence model, this wall function was established assuming that the ground friction velocity u_* was equal to the surface friction velocity $u_{\tau 0}$. For the viscous sub-layer:

$$u^+ = z^+ \quad (1)$$

here $u^+ = \frac{u_p}{u_\tau}$ is the dimensionless wall tangential velocity and the dimensionless height z^+ can be

expressed as $z^+ = \frac{u_\tau z_p}{\nu}$, where u_τ , z_p , ν and κ stand for the friction velocity ($= \sqrt{\frac{\tau_w}{\rho}}$), the distance from the

wall adjacent cell centre to the wall surface, kinetic viscosity and Kármán constant (≈ 0.4), respectively.

Note that the hybrid RANS/LES method, as reference [20] pointed out, was deployed to simulate the turbulent flow over the complex terrain. In the RANS region, the logarithmic law-of-the-wall was used as the wall-function to determine the wall shear stress based on the instantaneous tangential velocity of the first off the wall grid point. In contrast, a user-defined wall function referred in [21] for the near-wall treatment, based on the sub-layer tangential velocity, was utilized in this paper, which should improve the accuracy of the shear stress computation and thus the simulation of the flow field near the wall surface to some extent. On the other hand, for the high Reynolds number flow case, the present wall treatment method normally showed little difference with the classical logarithmic one. Nevertheless, considering the high turbulence intensity (around 20% at nominal hub height of 70 m) of the inlet cyclone flow as well, fluctuating velocity field tended to become more difficult to be accurately described, especially within the near wall region. To this end, the User Defined Function (UDF) to resolve the sublayer above the double hill surface, with a finer grid density, had been deployed to improve the accuracy of the computation. Moreover, a standard RANS model with the improved model constants was used and a much reduced computational cost was acquired than the hybrid RANS/LES method.

For the fully turbulent region:

$$u^+ = \frac{1}{\kappa} \ln\left(\frac{z_p}{z_0}\right) = \frac{1}{\kappa} \ln\left(\frac{u_{\tau 0} z_p}{\nu z_0 u_{\tau 0}}\right) = \frac{1}{\kappa} \ln\left(z^+ \frac{\nu}{z_0 u_{\tau 0}}\right) = \frac{1}{\kappa} \ln\left(\frac{z^+}{z_0^+}\right) \quad (2)$$

here $z_0^+ = \frac{z_0 u_{\tau 0}}{\nu}$ is dimensionless roughness height of the ground.

As mentioned before, the CFD scheme was developed based on the commercial FLUNT software. The inlet flow was driven by the external force, following the given equations of the kinetic energy k and the dissipation rate ε , while the free outflow condition was set at the outlet of the computation zone. For other boundaries, including top and side ones, the free-velocity conditions were assumed. To allocate fine mesh regions near the ground and to make the vertical grid lines straight, the individual vertical growth rates of the grid distribution were 1.10 and 1.02 in and out of the boundary layer flow above the double hill. To further improve the accuracy of computation, the cells of 1st layer were located in the sub-layer region, *i.e.*, $z^+ < 5$, so that the grid density was greatly enhanced near the hill surfaces to deal with the complex flow separation phenomena. Based on the grid independence test, the average grid resolution of $1,030 \times 590$ was used. In addition, the finite-volume discretization in the boundary-fitted coordinates, the SIMPLEC algorithm to couple pressure and velocity on a non-staggered grid and the QUICK scheme for the convection terms, were utilized to further improve the accuracy of the calculation.

It was also worth to mention that, using the CFD scheme, the construction of a good equilibrium flow in the present paper was not an easy task and we made a lot of efforts by adjusting our CFD scheme. Even so, the horizontal equilibrium of the resulting flow was not perfectly achieved, especially for the long-distant turbulent evolution along the streamwise direction, but it was not the case for the regions around the presently investigated double hill models under all incoming conditions, which had been tested in terms of mean and turbulent quantities (not shown) before the double hill models were put into the computation domain.

To verify the developed CFD method, we used the same situation, *e.g.*, incoming flow condition and test models, as the experiment by Kim *et al.* [4]. Interested readers may consult reference for the details of the experiments.

The longitudinal log-law velocity distribution, $U_z = \frac{u_*}{\kappa} \ln(\frac{z}{z_0})$, with the friction velocity $u_* = 0.33$ m/s and the aerodynamic roughness height $z_0 = 0.05$ mm, was set at the inlet of the computation zone, mimicking a neutrally stratified boundary layer. The corresponding kinetic energy k_z and dissipation rate ϵ_z were expressed as in the reference [4]:

$$k_z = (\overline{u_z^2} + \overline{v_z^2} + \overline{w_z^2})/2 \tag{4}$$

$$\epsilon_z = -\overline{u_z w_z} \frac{\partial U_z}{\partial z} \tag{5}$$

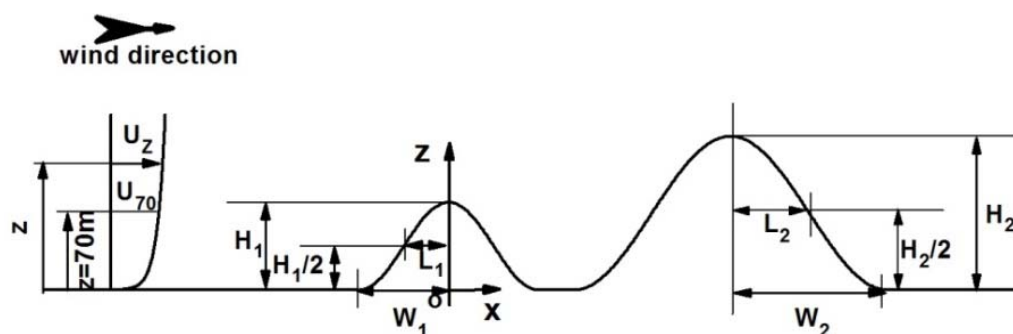
here u , v and w stand for the longitudinal, lateral and vertical fluctuating velocity, respectively.

Four double hill models, designated as S3H4-S3H7, S3H7-S3H4, S5H4-S5H7 and S5H7-S5H4, were utilized, which were composed of four single 2D symmetry hill models with various heights and slopes, individually labeled as S3H4, S5H4, S3H7 and S5H7. Each single hill has a profile given by:

$$z = \frac{H}{2} [1 + \cos(\frac{\pi x}{2L})] \tag{6}$$

where $S(=H/2L)$, H and L stand for the slope, the height and the half-width at the upwind mid-height of the single hill, respectively, shown in Figure 1.

Figure 1. Schematic computational domain of the wind flow over 2D double hill.



The coordinates x and z correspond to the streamwise and vertical direction, respectively, with the origin of the coordinate system located at the center of the upwind hill. Meanwhile, a subsidiary vertical coordinate (z') was used to express the height above the local hill surface. The symbols S3 and S5 represent the slope of 0.3 and 0.5, corresponding to non-separated and separated flow cases, while

H4 (=4 cm) and H7 (=7 cm) are the height of the hill. The distance between the upwind hill back and the downwind hill foot is 5 cm. The zenith of the first hill is $7H_7$ from the inflow boundary, and the computational domain extends $7H_7$ behind the zenith of second hill in x direction and $7H_7$ in z direction, respectively.

For the purpose of verification, the comparisons of CFD computation with the experimental results by Kim *et al.* were made in terms of mean and fluctuating turbulence flow. Figure 2 displays the typical longitudinal velocity profiles for all double hills. It is easy to note that, for non-separated cases, *i.e.*, S3H4-S3H7 (Figure 2a) and S3H7-S3H4 (Figure 2b), the numerical results agree very well with the experimental ones, while a little bit small differences exist for separated cases, *i.e.*, S5H4-S5H7 (Figure 2c) and S5H7-S5H4 (Figure 2d), especially within the regions of separated flow behind the downwind hill. Figure 3 shows the streamwise variations of normalized turbulence kinetic energy (k) profile for single S3H7 hill. Clearly, compared with experimental results, the general trend of k with z' was almost reproduced by computation.

Figure 2. Vertical profiles of mean longitudinal velocity over the double hills: (a) S3H4-S3H7; (b) S3H7-S3H4; (c) S5H4-S5H7; (d) S5H7-S5H4 (symbol, experimental data; line, computational fluid dynamics (CFD) results).

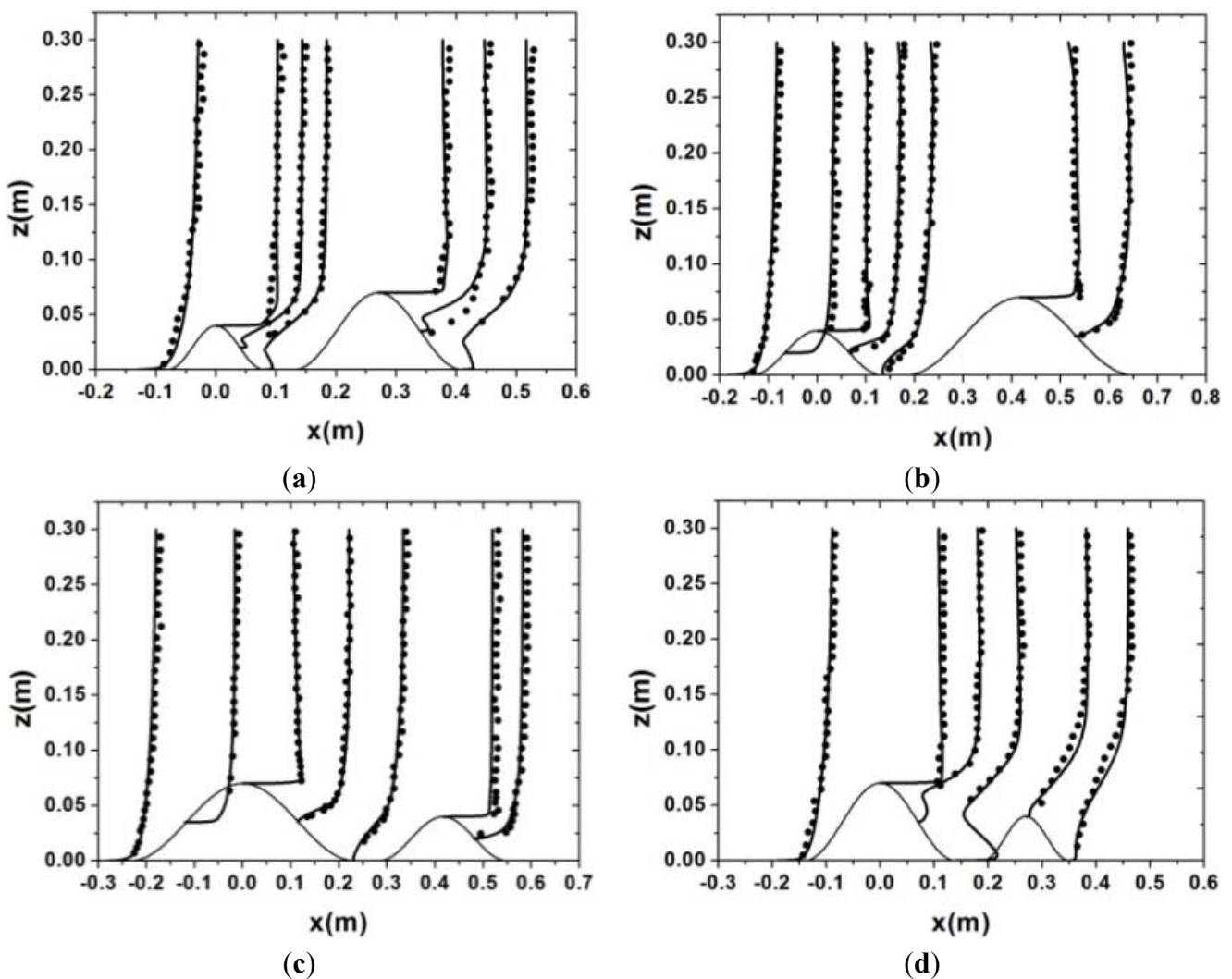
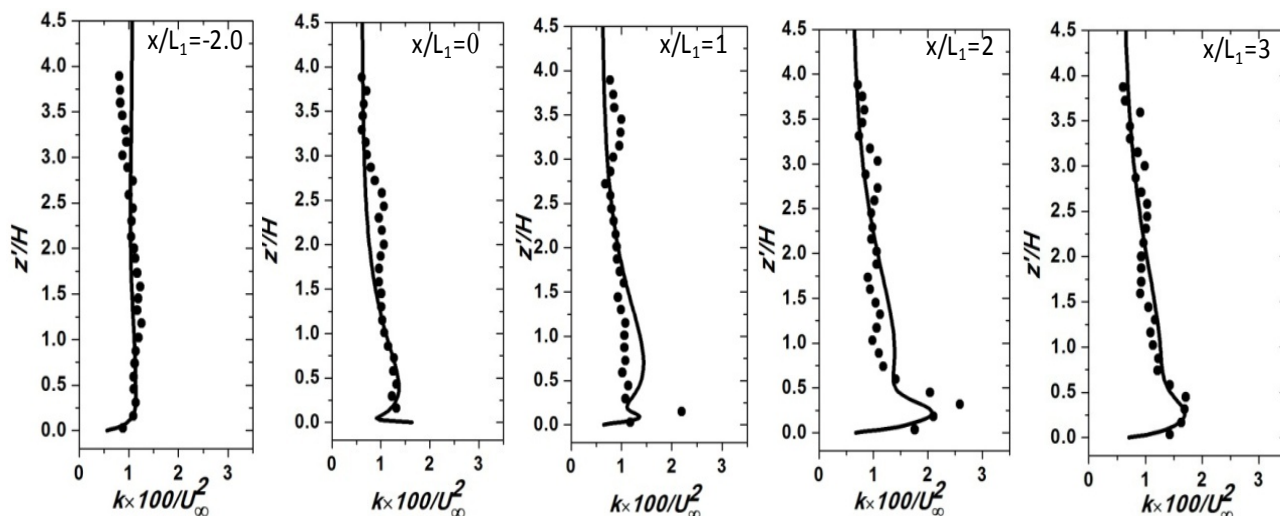


Figure 3. Comparison of predicated and measured turbulence kinetic energy profiles over single hill S3H7 (symbol, experimental data; line, CFD results).



From these results, the developed CFD algorithm was verified and it would be deployed in the following sections, since the turbulent flow of the cyclone is of similar order of Re (based on hill height, around 10^5) as those in Kim *et al.* [4]. By doing so, it might cause some unnecessary errors during the analysis of the flow field in a very specific way. However, considering the fact that the present research interest was mostly focused on the statistic characteristics of the cyclone effect, this deviation would not change the main conclusions of the paper.

3. Cyclone Effect the Flow over 2D Continuous Rolling Hills

3.1. Incoming Cyclone Flow

As mentioned before, it was very necessary to investigate the effect of the cyclones on the turbulent flow over rolling hills based on the field test data. For this reason, we analyzed the cyclone data within southeast coastal area from 1949 to 2010 [22] and we found that the beneficial and destructive cyclones accounted for almost 85% of all cyclones in the past 60 years; the wind speed profiles for the two cases generally abided by the power law equation with the average exponents α of 0.18 and 0.14, respectively:

$$U_z = U_{hub} \left(\frac{z}{z_{hub}} \right)^\alpha \tag{7}$$

In addition, the 10 min-field data for typical 29 cyclones and 88 anemometer towers since 2003, was also analyzed statistically, leading to a curve-fitted 5th interpolation function representing the variation of the mean turbulence intensity (I_{hub}) with the wind velocity U_{hub} at $z_{hub} = 70$ m:

$$I_{hub} = -0.90e^{-7}U_{hub}^5 + 0.98e^{-5}U_{hub}^4 - 0.42e^{-3}U_{hub}^3 + 0.87e^{-2}U_{hub}^2 - 0.96e^{-1}U_{hub} + 0.70 \tag{8}$$

From these analyses, the typical beneficial and destructive cyclones, corresponding to U_{hub} of 20 m/s (wind scale 7, tropical depression) and 50 m/s (wind scale 12, typhoon), respectively, were selected as the incoming flow condition for the present investigations. Moreover, using the $k-\epsilon$ model, the forms of

the inlet distributions of kinetic energy (k_z) and dissipation rate (ε_z), presented using Equations (9) and (10), were often adopted for the calculation:

$$k_z = a(U_z I_z)^2 \quad (9)$$

$$\varepsilon_z = C_\mu^{3/4} \frac{k_z^{3/2}}{L_z} \quad (10)$$

where the integration turbulent length L_z , following the EU standard [23], and the turbulence intensity [24] were:

$$L_z = 300 \left(\frac{z}{300} \right)^{0.46+0.074 \ln z_0} \quad (11)$$

$$I_z = 1.11 \times 35^{1.8(\alpha-0.16)} \left(\frac{z}{10} \right)^{-\alpha} / 2g, g = 2.2. \quad (12)$$

here $z_0 (=0.4)$ is the roughness height for the incoming flow and L_z , in the form of the verified version in Solari [25], depends on the minimum height and the power law exponent for the boundary layer of the terrain category in question.

Using the similar method in Sørensen [26], we have maintained the equilibrium of the flow. First, different previously verified standard equations of the turbulent length scale L_z were tested and the final EU version in Solari [25] was chosen due to its good application in the extreme wind condition. Based on this, L_z was equivalent to be prescribed. Then the transport equations of the turbulence model were modified in terms of the adjustment of the corresponding model coefficients. To guarantee the stability of the model equations, we chose the verified classical two-equation high Reynolds number $k-\varepsilon$ model in the reference [20] with improved empirical coefficients. In addition, the coefficient $a (=1.5)$ of the Equation (9) was also subject to the adjustment for many times before settling down. Even so, as mentioned before, the horizontal equilibrium of the resulting flow was not perfectly achieved, especially for the long-distant turbulent evolution along the streamwise direction, but the homogeneity of the flow within the investigated region was obtained to some degree.

The profile of the turbulence intensity distribution described by Equation (12) was acquired by Chinese researchers based on the long-term field test of tropical cyclones within the southeast coastal region, which reflected the main features of the tropical cyclones and was then chosen as the one of the boundary conditions to investigate the cyclone effect on the double hilly flow. Using Equation (12), I_{70} at $z_{hub} = 70$ m were individually calculated to be 0.202 and 0.169 for the two typical beneficial and destructive cyclones, while they were 0.204 and 0.160 if Equation (8) was applied, emphasizing the more rationality of Equation (12) for investigating the effect of cyclones on turbulent flow over continuous hills in China. Additionally, since the practical tropical cyclones generally took effect within a much larger area than that presently investigated and the two-dimensional statistical characteristics of cyclone flow were mainly studied in the paper, the variation in the wind direction was omitted and the incoming flow was assumed to move only in the streamwise direction.

3.2. Typical Beneficial and Destructive Cyclone Effect

Since separated flow phenomena over continuous hills are very common in practice, two double hill cases with higher slope, *i.e.*, S5H4-S5H7 and S5H7-S5H4, were thoroughly investigated.

A model/field scale of 1:4000 was used to give the equivalent hill height of 160 m and 280 m for the two single hills, *i.e.*, S5H4 and S5H7, representative of the typical height of rolling hills within the southeast coastal area in China. The roughness height z_0 was also assumed to be 0.4 to represent the typical feature of vegetations over model hill surface.

Figures 4 and 5 indicate the distributions of the streamwise velocity field and the kinetic energy field over the double hills under the influence of the typical beneficial and destructive cyclones, which seems to be much more drastic than normal wind condition reported by previous research. For the beneficial case, the wind velocity (U) over the two hills (Figure 4a,b) tends to be significantly increased, in contrast to the incoming cyclone flow, and U reaches the maximum above the top of the higher S5H7 hill. The flow separation is easily seen either in the valley of the two hills or behind the downwind hill. Meanwhile, it is noted that the flow over the higher S5H7 hill is little influenced by the upwind or downwind lower S5H4 hill, whereas those over S5H4 hill are greatly affected by the neighboring S5H7 hill so that the reverse flow behind the downwind S5H4 hill is almost invisible.

Figure 4. Distributions of streamwise velocity (U) field and kinetic energy (k) field over the double hills under the influence of the incoming beneficial cyclone: (a) U -field, S5H4-S5H7; (b) U -field, S5H7-S5H4; (c) k -field, S5H4-S5H7; (d) k -field, S5H7-S5H4.

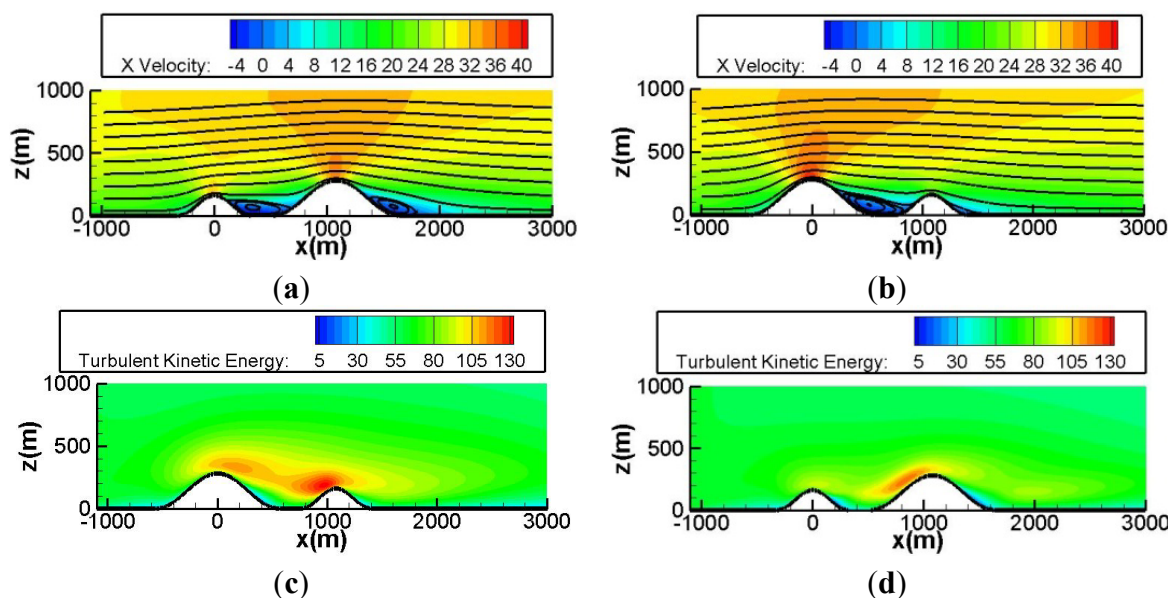


Figure 5. Distributions of streamwise velocity (U) field and kinetic energy (k) field over the double hills under the influence of the incoming destructive cyclone: (a) U -field, S5H4-S5H7; (b) U -field, S5H7-S5H4; (c) k -field, S5H4-S5H7; (d) k -field, S5H7-S5H4.

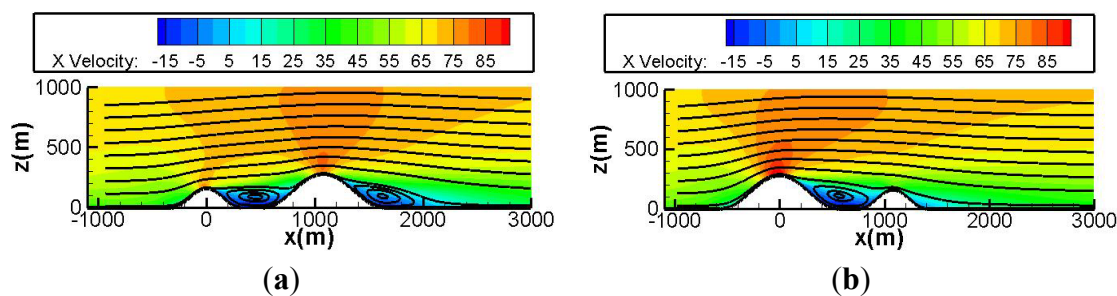
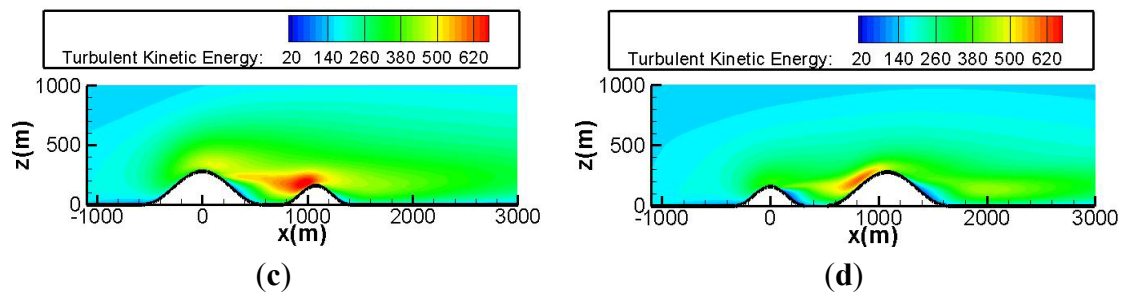


Figure 5. Cont.



This is associated with the increased turbulence at the downwind S5H4 hill crest from the separation of the upwind S5H7 hill, leading to the effective impairment of the detachment from the downwind S5H4 hill. Correspondingly, the flow reattaches to the ground much quicker behind downwind S5H4 hill than that behind downwind S5H7 hill, attributed to the fact that the flow momentum for the latter is much smaller than the former and thus the reattachment bubble may extend further downstream until the flow returns to a fully turbulent state. Here the mean reattachment location was determined to be the nearest grid point to the wall where $U = 0$. The turbulent kinetic energy k , produced by the mean strain rates (mainly by streamwise and lateral fluctuating velocity), is greatly enhanced over the double hill area and then generally smoothed out by the viscous dissipation as the flow moves toward downstream (Figure 4c,d). Clearly, the recovery of k -field to the undisturbed condition may extend to a longer distance than that of U -field. The magnitude in k reaches the local maximum around the height of each single hill, but near the top rear of the upwind hill and the top front of the downwind hill, respectively, and the latter is a little larger than the former, apparently due to the flow separation from the upwind hill. Figure 5 exhibits the U - and k -fields under the effect of the destructive cyclone. In general, the similar phenomena with its beneficial counterpart happen again except for the much stronger flow separation induced by the double hills and 2–5 times higher in the largest magnitude of U and k . To further evaluate the specific status of cyclone flow over double hills, the vertical profiles of the mean and fluctuating quantities at five typical positions of each hill, together with two leeside locations of the corresponding single hill, were calculated and displayed in Figures 6–9.

Figure 6 shows the results of fractional speed-up ratio S , defined by [8]:

$$S = \frac{U_{z'} - U_0}{U_0} \quad (13)$$

where $U_{z'}$ is the wind speed at height z' above the local surface of the hill and U_0 is the reference wind speed at the same height above the flat surface. In fact, Equation (13) relates the increase in wind speed at a given height to the undisturbed wind speed at the same height above the surface. It is interesting that the vertical variation in S seems very similar for beneficial and destructive cyclone cases. The distinct speed-up phenomena occur at the crests of the double hill, with the maximum S of 0.7–1.1 near the hill surface. At $z' = 70$ m (nominal hub height), S at the hill crest lies in a range of 0.4–0.7 except the downwind S5H4 hill for the S5H7-S5H4 hill case, where S is near zero (Figure 6d,h), consistent with the observations in Figures 4b and 5b.

Figure 6. Variation of fractional speed-up ratio with height z' over the typical positions of S5H4-S5H7 and S5H7-S5H4 hills for two cyclone cases: (a) beneficial, upwind S5H4 hill; (b) beneficial, downwind S5H7 hill; (c) beneficial, upwind S5H7 hill; (d) beneficial, downwind S5H4 hill; (e) destructive, upwind S5H4 hill; (f) destructive, downwind S5H7 hill; (g) destructive, upwind S5H7 hill; (h) destructive, downwind S5H4 hill.

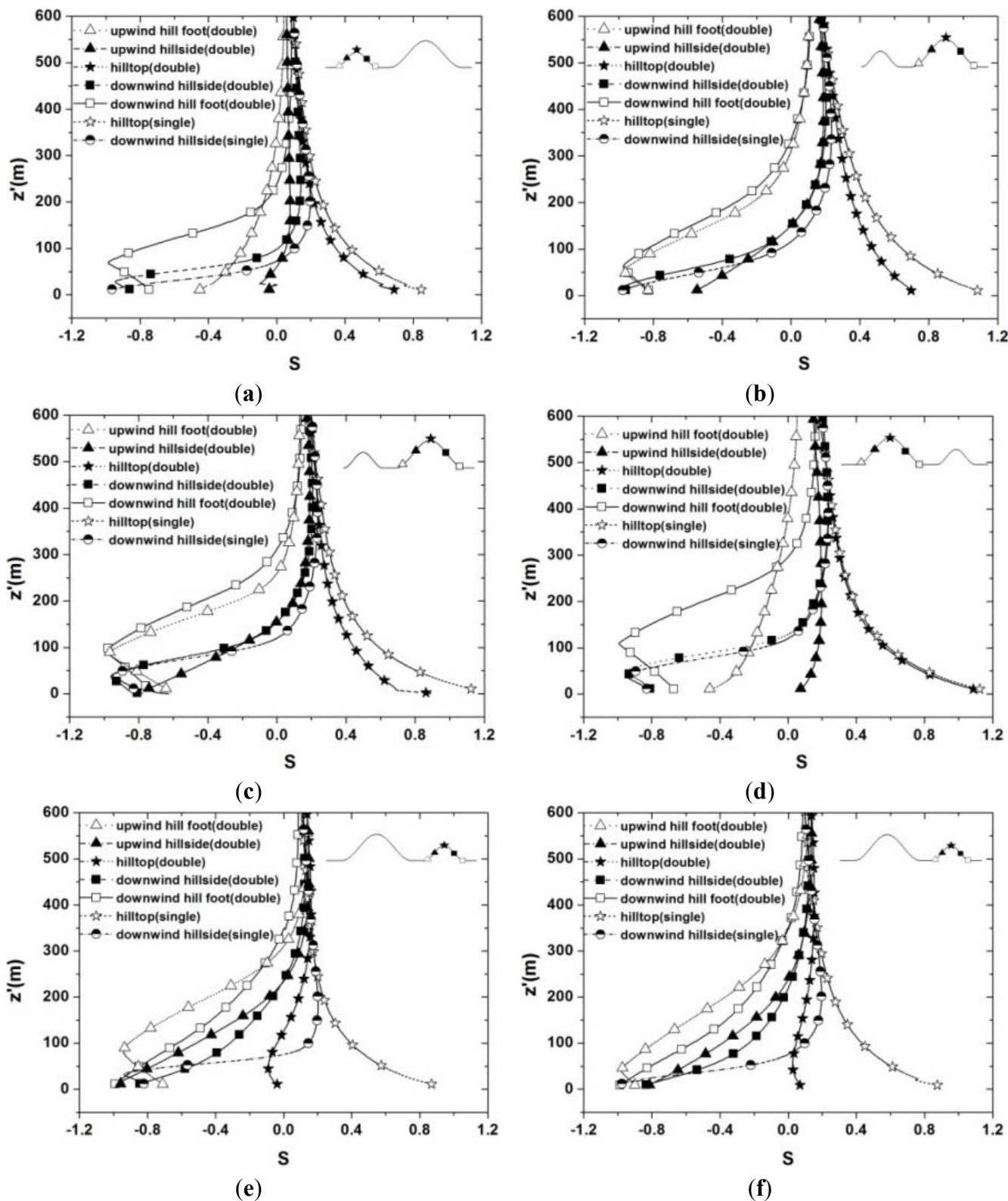
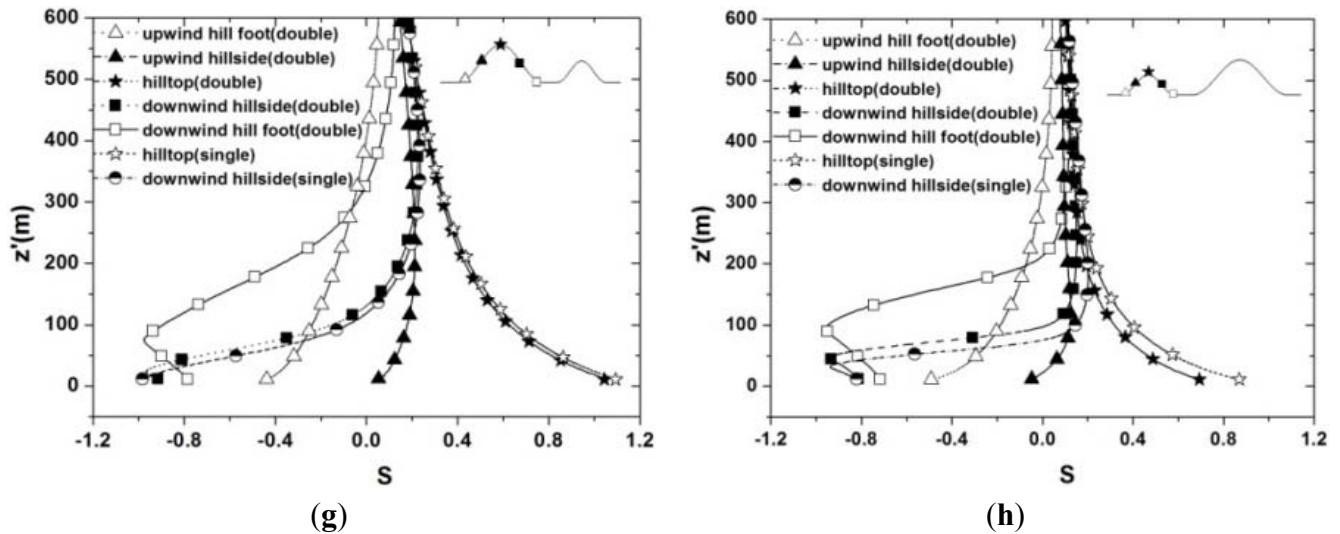


Figure 6. Cont.



Because of the influence of the neighboring hill, the speed-up ratio over the double hill top is found to be smaller than that at the single hill top. The momentum loss due to the adverse pressure gradient and viscous dissipation in the separation regions between the hills and behind the second hill are thought to be responsible for this, which may be also deduced from the results in Figures 4 and 5. Additionally, it is also noted that the wind speed at most of other locations decreases (negative S) near the hill surface and S gradually increases with increasing z' to obtain a rather weak speed-up above a height of 500 m.

Moreover, the typical profiles of the Reynolds stress \overline{uv} on the crests of the S5H7-S5H4 hill and the corresponding single hills, normalized by the value at the same height above the ground, \overline{uv}_r , also clarifies the difference between them, shown in Figure 7. Here u and v correspond to the longitudinal and vertical velocity fluctuation, respectively. Clearly, the point with the maximum $\overline{uv}/\overline{uv}_r$ is located at a higher z' height for double hill case (especially for S5H4 hill case). This suggests that the inner layer expands upwards over double hill, leading to a higher position of the maximum $\Delta U (= U'_z - U_0)$ [4,8]. One may also see the upwind S5H7 hill takes much more effect on the flow over the downwind S5H4 hill, agreeable with those in Figures 4–6.

Figure 8 presents the vertical profiles of turbulence intensity $I_{z'}$ ($=\sigma/U_{z'}$), where σ is the standard deviation of longitudinal velocity fluctuation. Although the incoming destructive cyclone flow causes $I_{z'}$ to be larger in magnitude and more tremendous in fluctuation at the same height than the beneficial case, both of them increase with increasing z' until $z' = 50\text{--}150$ m, possibly due to the great enhancement in k (Figures 4 and 5), and then quickly decrease to almost collapse on a single curve as $z' > 400$ m. The maximum $I_{z'}$ individually lies in the range of 0.25–0.30 for the beneficial case and 0.22–0.32 for the destructive case. The two neighboring hills influence with each other, leading to much different results. For the upwind hill (Figure 8a,c,e,g), $I_{z'}$ gradually augments from the foreside to the leeward side of the hill; compared with the single hill case, $I_{z'}$ becomes smaller above the top and downwind hillside positions for the upwind lower hill, while they change a little for the upwind higher hill. For the downwind hill (Figure 8b,d,f,h), because of the combined flow separations from the double hill, $I_{z'}$ first reduces over the hill foreside and then rises over the hill leeward side; In contrast with the single

hill case, I_z' tends to be smaller and larger over the leeside of the downwind higher and lower hill, respectively.

Figure 7. Variation of Reynolds stress with height z' over the hill top positions of S5H7-S5H4 hill and corresponding single hills for two cyclone cases: (a) S5H7 hill; (b) S5H4 hill.

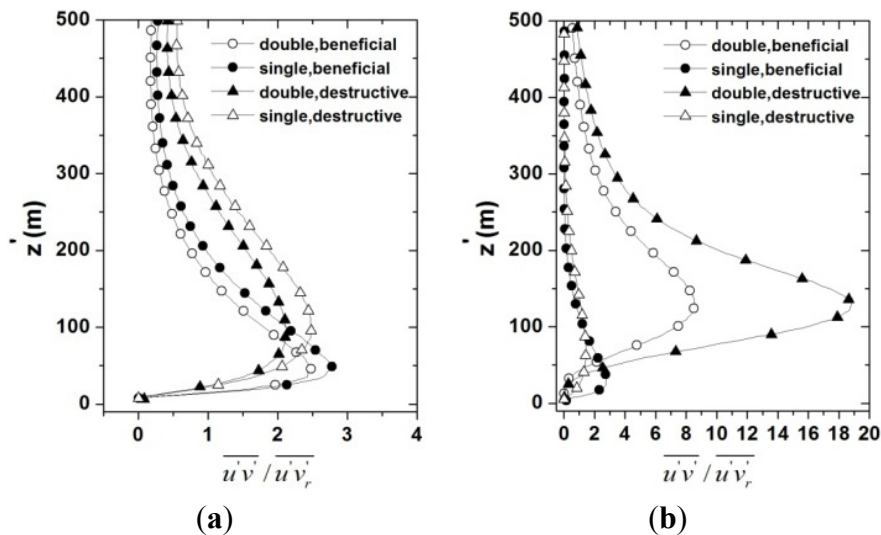


Figure 8. Variation of turbulence intensity with height z' over the typical positions of S5H4-S5H7 and S5H7-S5H4 hills for two cyclone cases: (a) beneficial, upwind S5H4 hill; (b) beneficial, downwind S5H7 hill; (c) beneficial, upwind S5H7 hill; (d) beneficial, downwind S5H4 hill; (e) destructive, upwind S5H4 hill; (f) destructive, downwind S5H7 hill; (g) destructive, upwind S5H7 hill; (h) destructive, downwind S5H4 hill.

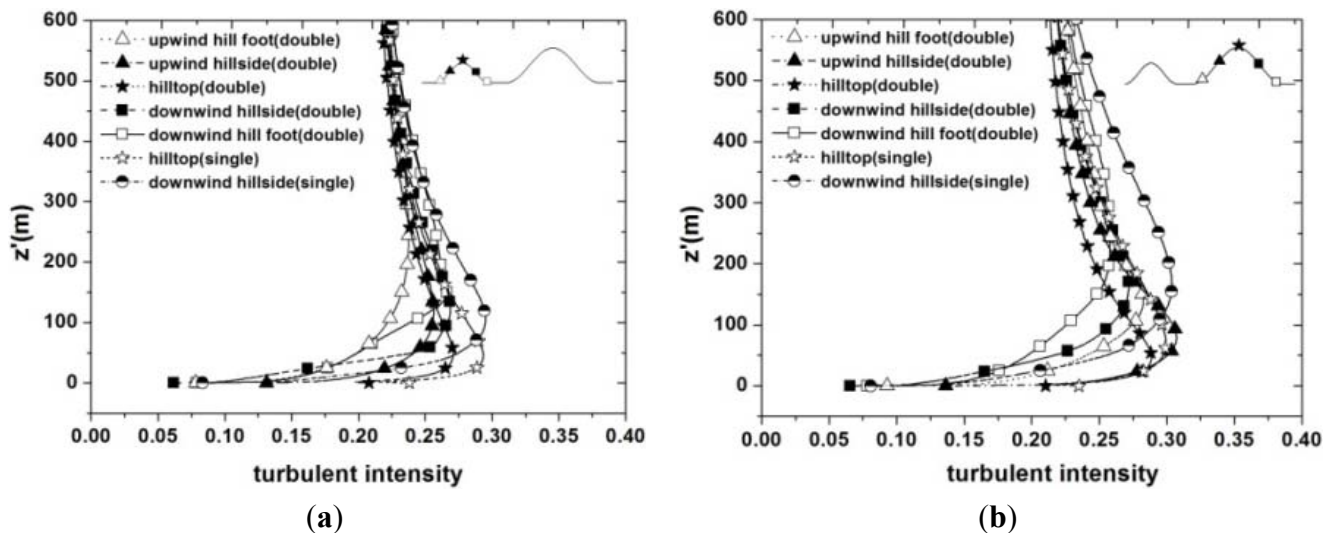
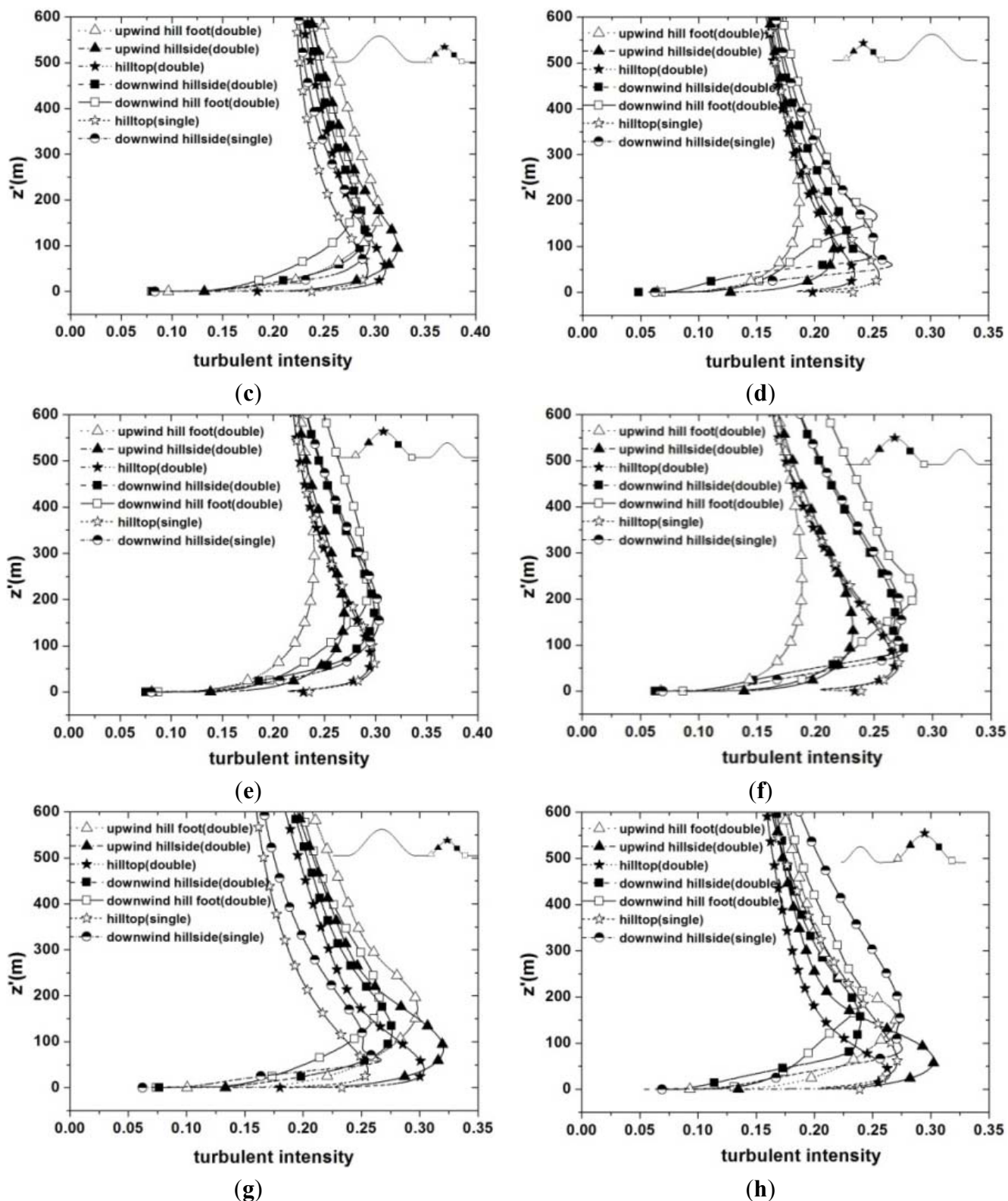


Figure 8. Cont.



Considering the importance in the normal wind resource evaluation, the mean gust speed $U_{gz'}$ along z' direction was calculated using the following equation [14]:

$$U_{gz'} = U_z (1 + gI_z) \tag{14}$$

here the peak factor g is 3.7. Furthermore, the gust speed ratio $G (= \frac{U_{gz'} - U_{g0}}{U_{g0}})$ was selected for the purpose of comparison, where $U_{gz'}$ and U_{g0} represents the gust speed at same height above hill surface and flat ground, respectively. Figure 9 gives a series of G -profiles for different single and double hill cases. Interestingly, the general features of G -profiles were very similar with S -profiles, irrespective of beneficial and destructive cases. Compared with other locations, the magnitude of G is much larger at hill top, especially on the crest of S5H7 hill, reaching the maximum value of 1.6 near the hill surface and 0.9 at $z' = 70$ m. Even so, the gust speed ratios over the hill top and downwind hillside are still smaller than those above the corresponding undisturbed single hills.

Figure 9. Variation of gust speed ratio with height z' over the typical positions of S5H4-S5H7 and S5H7-S5H4 hills for two cyclone cases: (a) beneficial, upwind S5H4 hill; (b) beneficial, downwind S5H7 hill; (c) beneficial, upwind S5H7 hill; (d) beneficial, downwind S5H4 hill; (e) destructive, upwind S5H4 hill; (f) destructive, downwind S5H7 hill; (g) destructive, upwind S5H7 hill; (h) destructive, downwind S5H4 hill.

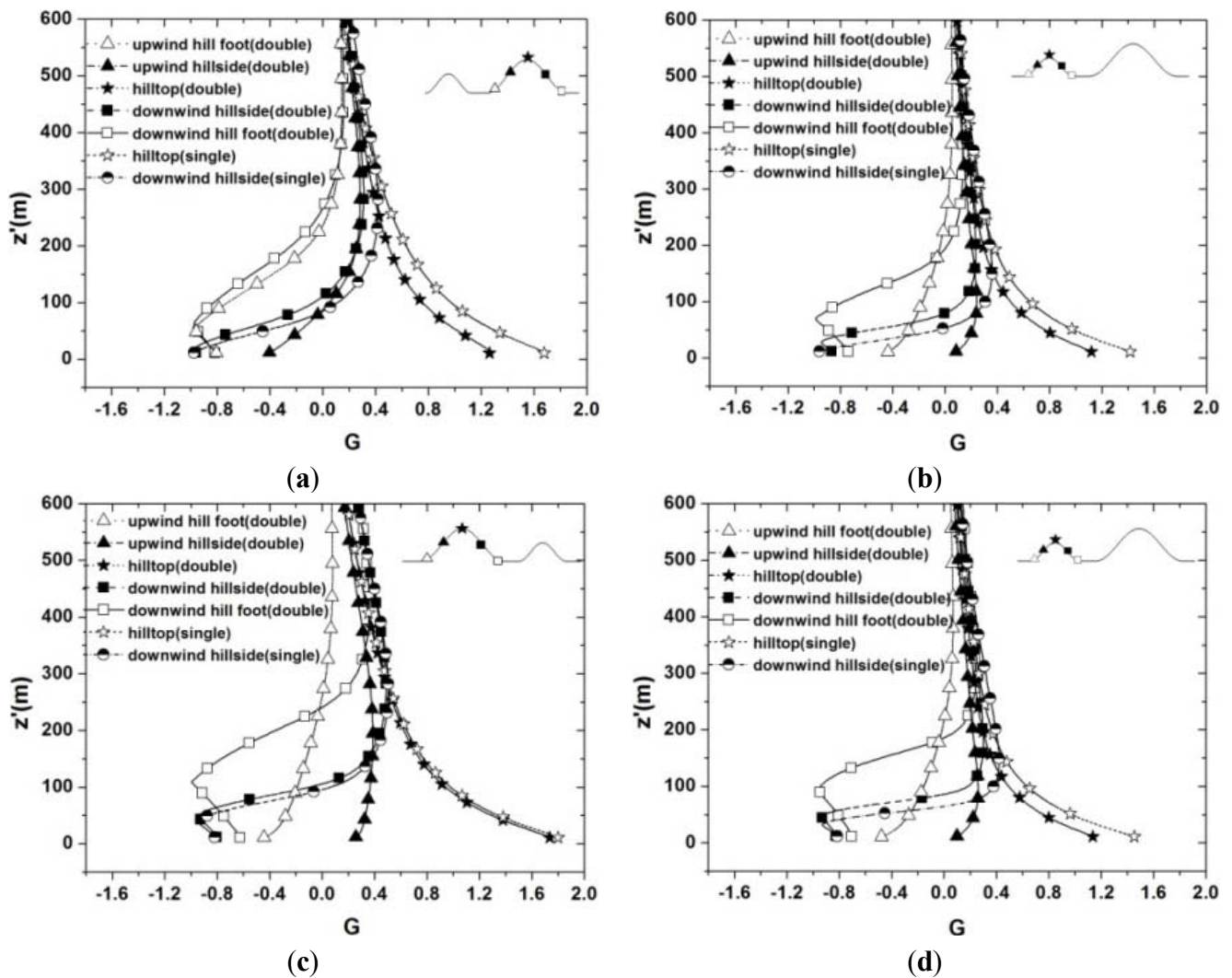
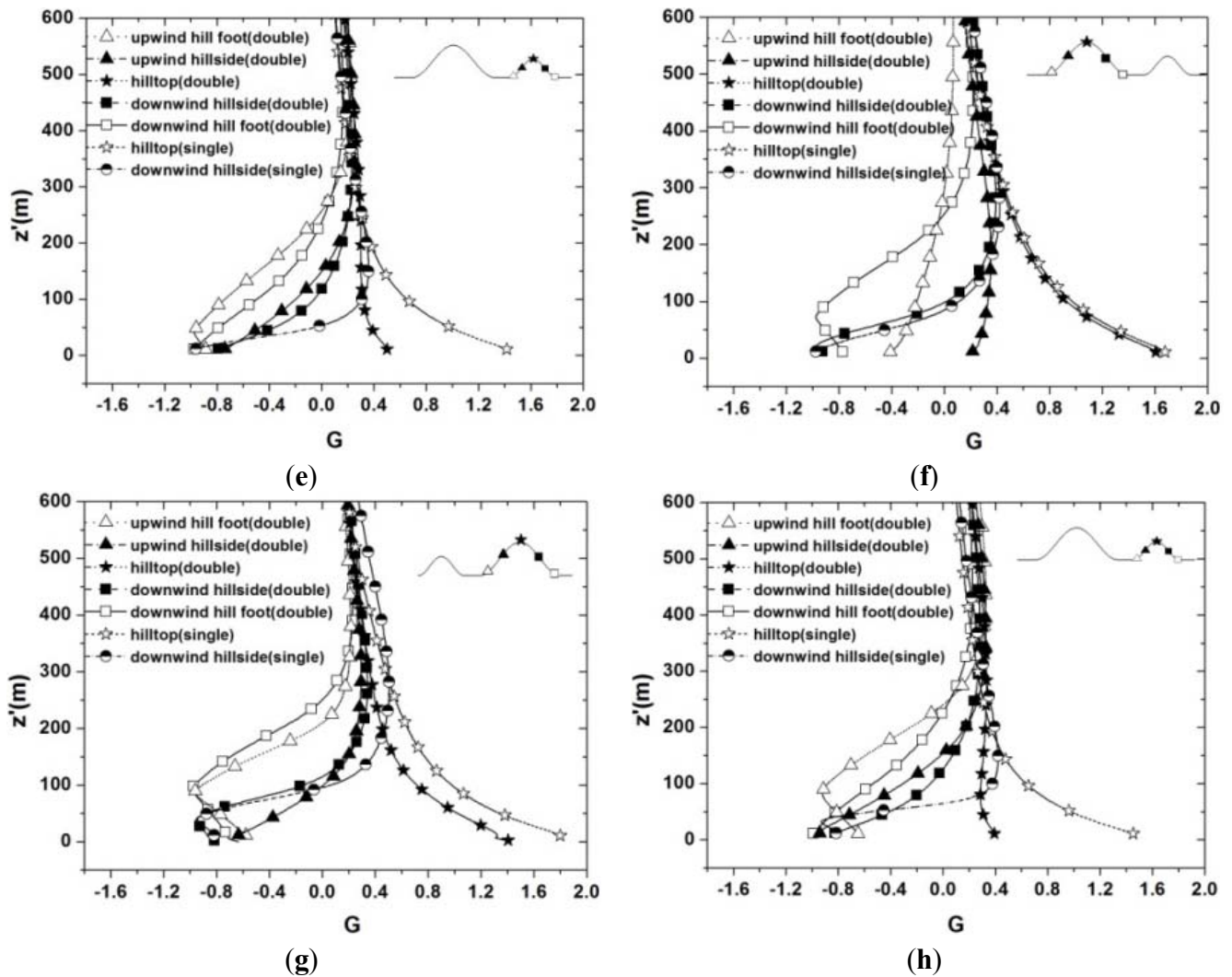


Figure 9. Cont.



3.3. Comparison of Cyclone Characteristics Based on Field Test Analysis and IEC Standard

As we know, the wind characteristics of tropical cyclones are not explicitly regulated in the IEC standard, the most widely accepted one for wind turbine design. Instead, people often deploy the existing IEC standard equations to approximately evaluate the cyclone flow. This undoubtedly makes it very difficult to obtain a cost effective and safe design under these conditions. To illustrate the difference in the wind evaluation results based on IEC standard and our field test analysis in Section 3.2, the vertical profiles of flow over the top of the double hill were compared as a typical example, where the wind energy utilization was regularly paid most attention.

It is worth mention that, for IEC case, the velocity profiles for the incoming beneficial and destructive cyclone flow were still expressed using Equation (4), except that α was 0.20 and 0.11, respectively, following with the standard equations of IEC Normal Turbulence Model (NTM) and IEC Extreme Wind Model (EWM) [18]. In addition, Equation (15) [27] were employed to calculate I_z :

$$I_z = \begin{cases} 0.1\left(\frac{z}{z_g}\right)^{-\alpha-0.05}, & z_b < z < z_g \\ 0.1\left(\frac{z_b}{z_g}\right)^{-\alpha-0.05}, & z \leq z_b \end{cases} \tag{15}$$

here z_g (=650 m) and z_b (=5 m) are the height of gradient wind, where the wind velocity tends to be negligibly influenced by the ground roughness, and the characteristic height, respectively. It was reasonable since I_{70} based on Equation (15) was 0.175 and 0.143 for the two cyclones, while their counterparts were 0.165 and 0.141 using the following equations from IEC NTM and IEC Extreme Turbulence Model (ETM) [18]:

$$I_{Ben,70} = I_{NTM} = \frac{\sigma_{NTM}}{U_{hub}} = \frac{I_{ref}(0.75U_{hub} + 5.6)}{U_{hub}} \tag{16}$$

$$I_{Des,70} = I_{ETM} = \frac{\sigma_{ETM}}{U_{hub}} = cI_{ref}\left(0.072\left(\frac{U_{ave}}{c} + 3\right)\left(\frac{U_{hub}}{c} - 4\right) + 10\right) \tag{17}$$

here σ , I_{ref} , U_{ave} and c stands for the standard deviation of longitudinal velocity fluctuation, the expected value of turbulence intensity at 15 m/s (=0.16, assuming the highest turbulence level according to IEC standard), the annual average wind speed at hub height (=25 m/s for IEC Class I case) and a constant (=2 m/s), respectively.

Figures 10–12 show the compared $U_{z'}$ -, $I_{z'}$ - and $U_{gz'}$ -profiles over the crests of the S5H7-S5H4 hill. Similar results were also observed for the S5H4-S5H7 hill case and are not shown for simplicity. Figure 10 exhibits the vertical profile of wind velocity $U_{z'}$. For the beneficial cyclone case, $U_{z'}$ on the hill crest appears no discernible difference (Figure 10a,b). On the other hand, for the destructive cyclone case, the wind velocities using the IEC EWM model were underestimated by up to 19.0% and 33.3% over upwind S5H7 hill and downwind S5h4 hill, respectively, in contrast to the results based on the field test analysis.

Figure 10. Variation of wind velocity with height z' over the crests of S5H7-S5H4 hill for two cyclone cases: (a) beneficial, upwind S5H7 hill; (b) beneficial, downwind S5H4 hill; (c) destructive, upwind S5H7 hill; (d) destructive, downwind S5H4 hill.

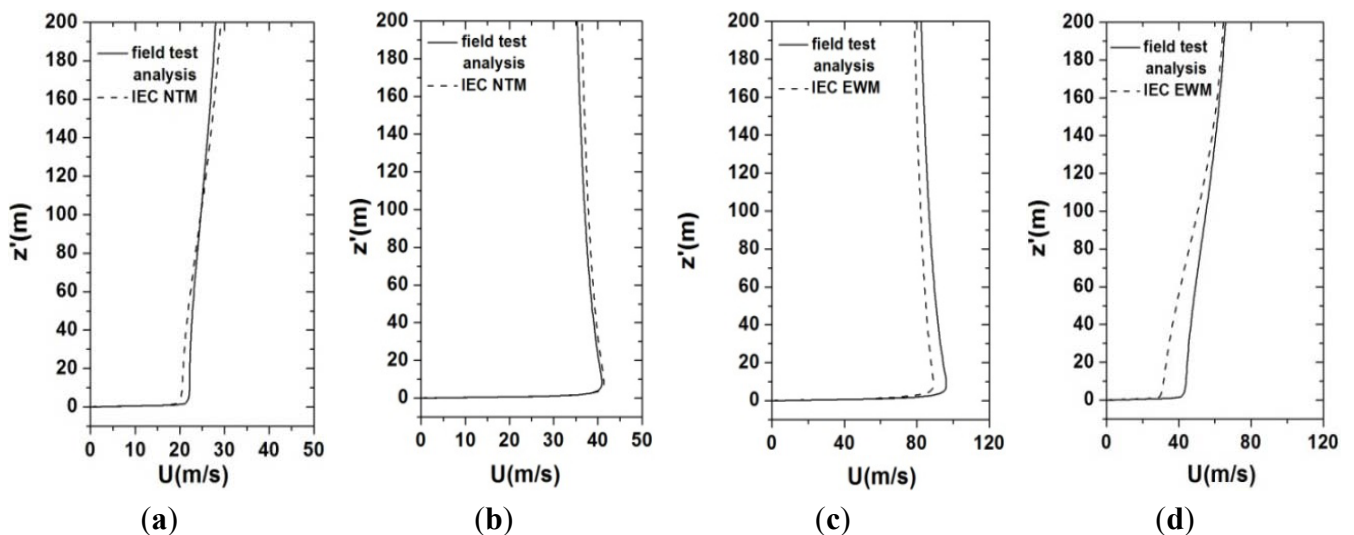


Figure 11. Variation of turbulence intensity with height z' over the crests of S5H7-S5H4 hill for two cyclone cases: (a) beneficial, upwind S5H7 hill; (b) beneficial, downwind S5H4 hill; (c) destructive, upwind S5H7 hill; (d) destructive, downwind S5H4 hill.

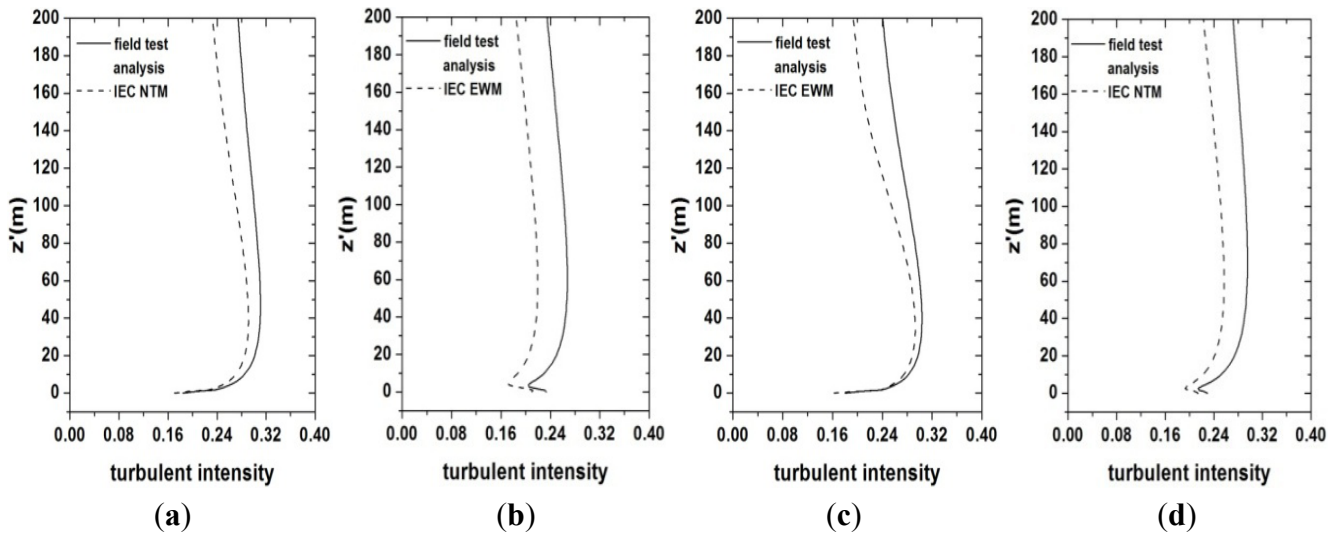


Figure 12. Variation of gust speed with height z' over the crests of S5H7-S5H4 hill for two cyclone cases: (a) beneficial, upwind S5H7 hill; (b) beneficial, downwind S5H4 hill; (c) destructive, upwind S5H7 hill; (d) destructive, downwind S5H4 hill.

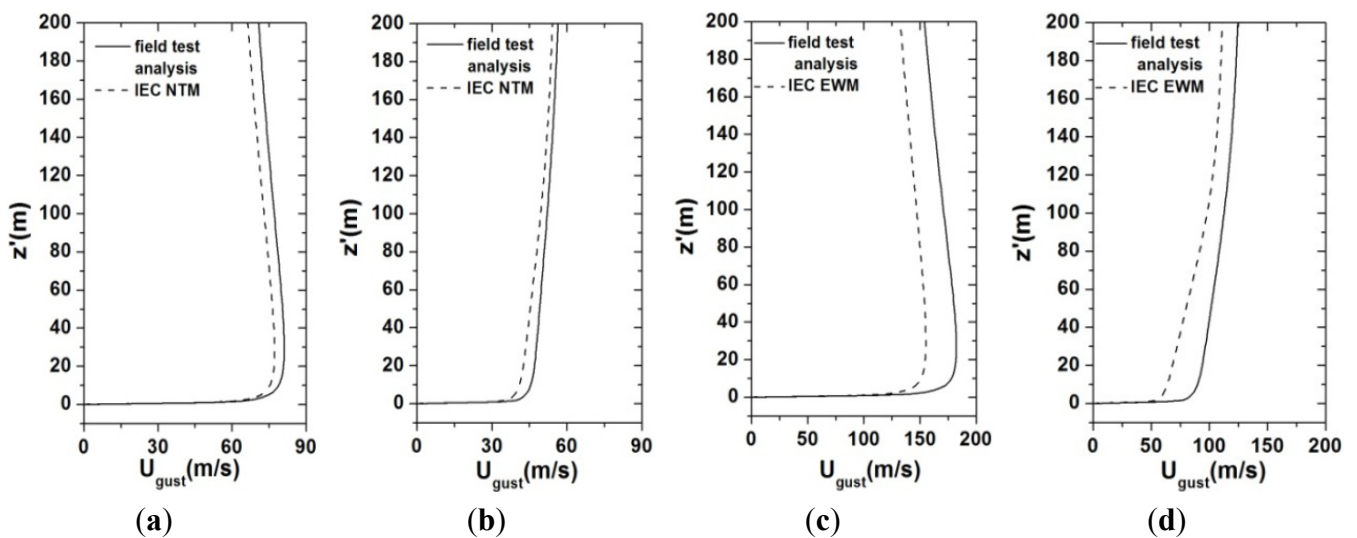


Figure 11 displays the variation of turbulence intensity $I_{z'}$ with z' . Evidently, using the incoming flow based on our field test analysis, $I_{z'}$ is always larger within the whole investigated z' range (0–200 m) than that based on IEC equations, regardless of any cyclone case, especially when the crest of the upwind S5H7 hill was concerned. At the hub height $z'_{hub} = 70$ m, the test data based I_{70} is about 0.26–0.31, which are 15.4%–27.3% higher than those calculated using IEC NTM and EWM models.

Figure 12 points out the difference in the gust speed $U_{gz'}$. Analogous to $I_{z'}$, $U_{gz'}$ tends to be smaller in case where the IEC standard were utilized and this was particularly true for destructive cyclone case. The maximum percentage of difference is up to 42.9% as $z' < 200$ m and it is up to 26.0% at z'_{hub} . To sum it up, the three quantities, $U_{z'}$, $I_{z'}$ and $U_{gz'}$, were generally much underestimated in case the IEC standard was utilized.

It was easy to note that, using the IEC standard, the magnitudes of the wind velocity, the turbulence intensity and the gust speed were evidently lower than those based on the field test analysis, especially for the destructive cyclone case. In fact, the turbulent flow separation around the double hills tended to be much stronger for the destructive cyclone case than the beneficial cyclone case, as illustrated in Figures 4 and 5. Furthermore, the difference in the turbulence intensity of the inlet flow between the field test analysis and the IEC standard for the former was also larger than that for the latter. Therefore, under the destructive cyclone condition, the flow detachment from the top of the hill would certainly be enhanced more based on the data obtained from the field test analysis than that based on the IEC standard, causing more distinctions in terms of the mean and fluctuating wind velocity. This would obviously lead to some problems concerned with the cost-optimization and fatigue load design of wind turbine and even micro-sitting of wind farm over complex terrain. For this reason, we strongly recommend introducing the wind shear and turbulence intensity formulas based on the field test analysis as a supplementary regulation into IEC standard for conducting more reasonable wind evaluations within the cyclone area in China.

4. Conclusions

This paper presented a numerical investigation of the effect of typical Chinese tropical cyclones on the turbulent flow over the 2D continuous hills using a developed CFD method. In addition, the representative results were also compared with those based on the IEC standard equations. Some conclusions could be drawn as follows:

- (1) The mean and fluctuating characteristics of double hilly flow due to tropical cyclones are generally much stronger and more fluctuant than the previously reported normal wind conditions;
- (2) Although rather intense flow separation occurs between and behind the two hills, the speed-up phenomena are very similar for beneficial and destructive cyclone case, resulting in: (a) the relative powerful speed-up appears at the crest of higher hill, with the maximum fractional speed-up ratio S of 0.7–1.1 and 0.4–0.7 at hub height ($=70$ m), respectively; (b) the flow field above the lower hill is much more influenced by the neighboring higher hill; (c) the S over double hill is found to be smaller than that above the corresponding single hill;
- (3) The turbulent quantities of destructive cyclones are much larger than those of beneficial cyclones in magnitude, but they tend to have similar features, mainly attributed to increased turbulence and momentum transport induced by the detachment of the hilly flow: (a) the kinetic energy k , the turbulence intensity I_z , and the gust-speed ratio G greatly fluctuate near hill surface, reaching their local maximum around the height of each hill, and gradually decrease with increasing hill height; (b) the maximum I_z around the hub height lies in the range of 0.22–0.32; (c) the G is much larger at hill top, reaching the maximum value of 1.6 near the hill surface and 0.9 at hub height;
- (4) In contrast to the field test analysis, both the averaged velocity and the turbulence strength over the representative hill tops are underestimated by up to more than 20% based on the IEC standard, which makes it very necessary to supplement the standard using the statistic field test formula for more reasonable wind evaluation within the southeast coastal area in China;

- (5) Using a similar method to Sørensen [26], together with the reasonable setting or adjustment of the integration turbulent length and the transport equations of the turbulence model, an approximate homogeneous turbulent flow over the double hills was acquired in the present paper. More numerical and experimental work was now underway to further improve this.

Acknowledgments

This work was supported by the National Natural Science Foundation of China (Grant No. 51076153).

Conflicts of Interest

The authors declare no conflict of interest.

References

1. Saucier, W.J. *Principles of Meteorological Analysis*; University of Chicago Press: Chicago, IL, USA, 1995; p. 415.
2. Burton, T.; Sharpe, D.; Jenkins, N.; Bossanyi, E. *Wind Energy Handbook*; John Wiley & Sons: Chichester, UK, 2001; pp. 215–217.
3. Bowen, A.J.; Lindley, D. A wind-tunnel investigation of the wind speed and turbulence characteristics close to the ground over various escarpment shapes. *Bound Layer Meteor* **1977**, *12*, 259–271.
4. Kim, H.G.; Lee, C.M.; Lim, H.C.; Kyong, N.H. An experimental and numerical study on the flow over two-dimensional hills. *J. Wind Eng. Ind. Aerodyn.* **1997**, *66*, 17–33.
5. Miller, C.A.; Davenport, A.G. Guidelines for the calculation of wind speed-ups in complex terrain. *J. Wind Eng. Ind. Aerodyn.* **1998**, *74–76*, 189–197.
6. Carpenter, P.; Locke, N. Investigation of wind speeds over multiple two-dimensional hills. *J. Wind Eng. Ind. Aerodyn.* **1999**, *83*, 109–120.
7. Takahashi, T.; Ohtsu, T.; Yassin, M.F.; Kato, S.; Murakami, S. Turbulence characteristics of wind over a hill with a rough surface. *J. Wind Eng. Ind. Aerodyn.* **2002**, *90*, 1697–1706.
8. Cao, S.Y.; Tamura, T. Experimental study on roughness effects on turbulent boundary layer flow over a two-dimensional steep hill. *J. Wind Eng. Ind. Aerodyn.* **2006**, *94*, 1–19.
9. Lubitz, W.D.; White, B.R. Wind-tunnel and field investigation of the effect of local wind direction on speed-up over hills. *J. Wind Eng. Ind. Aerodyn.* **2007**, *95*, 639–661.
10. Ngo, T.T.; Letchford, C.W. Experimental study of topographic effects on gust wind speed. *J. Wind Eng. Ind. Aerodyn.* **2009**, *97*, 426–438.
11. Xu, D.P.; Ayotte, K.W.; Taylor, P.A. Development of a non-linear mixed spectral finite difference model for turbulent boundary-layer flow over topography. *Bound Layer Meteor* **1994**, *70*, 341–367.
12. Taylor, P.A. Turbulent boundary-layer flow over low and moderate slope hills. *J. Wind Eng. Ind. Aerodyn.* **1998**, *74–76*, 25–47.
13. Bowen, A.J. Modeling of strong wind flows over complex terrain at small geometric scales. *J. Wind Eng. Ind. Aerodyn.* **2003**, *91*, 1859–1871.
14. Lun, Y.F.; Mochida, A.; Murakami, S.; Yoshino, H.; Shirasawa, T. Numerical simulation of flow over topographic features by revised k - ϵ models. *J. Wind Eng. Ind. Aerodyn.* **2003**, *91*, 231–245.

15. Uchida, T.; Ohya, Y. Micro-siting technique for wind turbine generators by using large-eddy simulation. *J. Wind Eng. Ind. Aerodyn.* **2008**, *96*, 2121–2138.
16. Cao, S.Y.; Wang, T.; Ge, Y.J.; Tamura, Y. Numerical study on turbulent boundary layers over two-dimensional hills—Effects of surface roughness and slope. *J. Wind Eng. Ind. Aerodyn.* **2012**, *104–106*, 342–349.
17. Jafari, S.; Chokani, N.; Abhari, R.S. An immersed boundary method for simulation of wind flow over complex terrain. *J. Sol. Energy Eng.* **2012**, *134*, 011006:1–011006:12.
18. International Electrotechnical Commission (IEC). *IEC 61400-1 Wind Turbines—Part 1: Design Requirements*, 3rd ed.; IEC: Geneva, Switzerland, 2005; pp. 24–27.
19. Clausen, N.E.; Candelaria, A.; Gjerding, S.; Hernando, S.; Norgard, P.; Ott, S.; Johansen, N.J.T. *Wind Farms in Regions Exposed to Tropical Cyclones*. In Proceedings of the European Wind Energy Conference & Exhibitions, Athens, Greece, 7–10 May 2007; pp. 1–10.
20. Bechmann, A.; Sørensen, N.N.; Johansen, J.; Vinther, S.; Nielsen, B.S.; Botha, P. Hybrid RANS/LES method for high Reynolds number, applied to atmospheric flow over complex terrain. *J. Phys.* **2007**, *75*, 012054, doi:10.1088/1742-6596/75/1/012054.
21. Zhang, X.D. *CFD Simulation of Neutral ABL Flows*; Risø-R-1688 (EN); Risø National Laboratory for Sustainable Energy, Technical University of Denmark: Roskilde, Denmark, 2009.
22. Zhang, X.Z.; Yan, J.Y.; Yang, X.S.; Zhang, R.Y. *Effect of Typhoon on the Development of Wind Power in China and Strategy*; China Meteorological Press: Beijing, China, 2010; pp. 9–56. (in Chinese)
23. *Eurocode. 1: Basis of Design and Actions on Structures—Part 2–4: Actions on Structures-Wind Actions*; European Committee for Standardization: Brussels, Belgium, 1995.
24. Shi, Y.; Lu, W.; Zhong, Y. Investigation of Typhoon Structure within Shanghai Region. In Proceeding of 2nd National Academic Conference on Wind Effect, Shanghai, China, 1988; pp. 1–12. (in Chinese)
25. Solari, G. Gust buffeting. I: Peak wind velocity and equivalent pressure. *J. Struct. Eng.* **1993**, *119*, 365–382.
26. Sørensen, N.N. *General Purpose Flow Solver Applied to Flow over Hills*; Risø-R-827 (EN); Risø National Laboratory: Roskilde, Denmark, 2003.
27. Tamura, Y.; Asami, Y.; Kawai, H.; Marukawa, H.; Nakamura, O.; Ohkuma, T.; Okuda, Y.; Ueda, H.; Uematsu, Y.; Kawabata, S. *et al.* Wind Loads. In *AIJ Recommendations for Loads on Buildings*; Architecture Institute of Japan: Tokyo, Japan, 2004; pp. 14–16.